*photonics*

MDPI

*Article*

# Photo-Modulation and Phase Behavior of Liquid Crystal Composites Based on Cyclic Diazobenzene Molecular Switches

**Tao Sun [1], Baiqing Zhang [1], Nijie Sheng [1], Yutong Wan [1], Hongzhao Sun [1,2,*], Chunlan Ma [1], Zhaoliang Cao [1] and Huanjun Lu [1,*]**

[1] Advanced Technology Research Institute of Taihu Photon Center, School of Physical Science and Technology, Suzhou University of Science and Technology, Suzhou 215009, China
[2] Key Lab of Nanodevices and Applications, Suzhou Institute of Nano-Tech and Nano-Bionics, Chinese Academy of Sciences, Suzhou 215123, China
* Correspondence: sunhongzhao@usts.edu.cn (H.S.); luhuanjun@usts.edu.cn (H.L.)

**Abstract**

Photochromic molecules, capable of reversible isomerization under specific light irradiation, are pivotal for developing advanced photo-responsive materials. Azobenzene derivatives, in particular, are renowned for their significant conformational change, excellent reversibility, and high photostability. This study presents a novel cyclic diazo compound (CDTA) comprising two azobenzene units connected via flexible glycol chains. The photo-responsive behavior of CDTA doped into the liquid crystal 4-cyano-4′-octylbiphenyl (8CB) was systematically investigated. The composite exhibits a pronounced photo-induced phase transition from a liquid crystalline to an isotropic state under 365 nm UV irradiation, accompanied by a reversible change in light transmittance. The response kinetics were found to be highly dependent on temperature and dopant concentration. At 35 °C, the UV response time was accelerated to 6.8 s, attributed to the transition of the host 8CB from a smectic to a nematic phase. Furthermore, the composite demonstrated dual responsiveness: optical switching under UV light and electrical switching under an applied field in its nematic state. This work elucidates the interaction between molecular structure and photo-response in a liquid crystalline matrix, offering insights for designing next-generation smart windows and adaptive optical devices.

**Keywords:** azobenzene; cyclic diazobenzene; liquid crystal; photo-responsive; phase transition

## 1. Introduction

Photochromic molecules, which undergo reversible isomerization between distinct states upon light irradiation at specific wavelengths, enabling switchable optical properties and functions, have garnered widespread interest for applications in optical memory, logic devices, molecular motors, and actuators [1–6]. Among these, azobenzene and its derivatives are particularly prominent due to the significant conformational change between the elongated *trans* and bent *cis* isomers, as well as excellent reversibility, and high photostability that endures numerous switching cycles [7–12]. Their ability to induce large-scale molecular reorientation and phase transitions in host systems, such as liquid crystals, further enhances their utility in advanced photo-responsive materials [13–16].

Owing to these advantages, azobenzenes have been extensively incorporated into light-responsive devices, including smart windows [17–19]. For instance, Yoon et al. developed a photo- and thermo-responsive smart window by controlling the 3D molecular



Received: 25 February 2026
Revised: 10 March 2026
Accepted: 26 March 2026
Published: 28 March 2026

orientation of chiral liquid crystals using azobenzene-based alignment layers, enabling autonomous transparency switching under UV light and thermal stimuli [20]. Oh et al. designed a self-regulating infrared smart window using push–pull azobenzene-doped liquid crystals to modulate NIR reflectance based on ambient temperature and light intensity [21]. Tkachenko et al. investigated azobenzene-containing main-chain polymers for photoalignment of liquid crystals, demonstrating high-resolution patterning and stable birefringence [22]. These studies illustrate the critical role of azobenzene derivatives in enabling multifunctional, efficient, and adaptive optical systems through tailored molecular design and host-guest integration.

Beyond conventional linear derivatives, constrained azobenzene structures, such as cyclic oligomers, offer novel photophysical behaviors and enhanced steric influences that can significantly impact isomerization pathways and material performance [23–26]. The cyclic architecture imposes spatial restrictions on the azobenzene units, leading to altered photophysical behaviors, including modified absorption spectra, enhanced steric effects, and sometimes accelerated thermal relaxation [27–35]. These unique characteristics can significantly impact isomerization pathways and the efficiency of photo-induced perturbations in host matrices. Compared to their linear counterparts, cyclic azobenzenes often exhibit different isomerization kinetics and a more pronounced influence on the molecular packing of liquid crystals due to their bulkier and more rigid structure [36,37]. Despite these promising features, systematic studies on cyclic azobenzene derivatives as dopants in liquid crystal composites remain limited. In this work, a cyclic diazo compound comprising two azobenzene units connected via flexible glycol chains at the para-positions was synthesized, and its photoresponsive behavior when doped into liquid crystal 4-cyano-4′-pentylbiphenyl (8CB) was investigated. The phase transitions, photoisomerization kinetics, and light transmission properties of the composite system were thoroughly characterized to elucidate the interaction between molecular structure and photo response in a liquid crystalline matrix.

## 2. Materials and Methods

The cyclic diazo compound (CDTA) was synthesized according to a modified literature procedure under high-dilution conditions [38], yielding an orange flaky solid (see Supplementary Materials for details). The chemical structure and the corresponding $^1$H-NMR spectrum was shown in Figure 1. The host liquid crystal 4-cyano-4′-octylbiphenyl (8CB) was used as received. Composite mixtures were prepared with CDTA concentrations of 1.5 wt%, 2.0 wt%, and 2.5 wt% in 8CB by physical blending at elevated temperature followed by stirring for homogeneity.

Test cells were fabricated using two glass substrates (with or without ITO coating, Ningcui Optics, Nanjing, China) separated by 10 μm spacers. No alignment layers were applied. The homogeneous LC/CDTA mixtures were injected into the cells via capillary action at room temperature.

The composite samples were prepared by physical blending at an elevated temperature, followed by continuous stirring for over 24 h to ensure homogeneity. The resulting mixtures were then injected into non-aligned test cells with a 10 μm gap via capillary action at room temperature.

The intensity of the 365 nm UV light source used for photo-irradiation was 2 mW/cm$^2$, as measured by an optical power meter (PM100D, Thorlabs, Newton, MA, USA). The recovery process was carried out under standard ambient room lighting with an intensity of approximately 0.5 mW/cm$^2$.

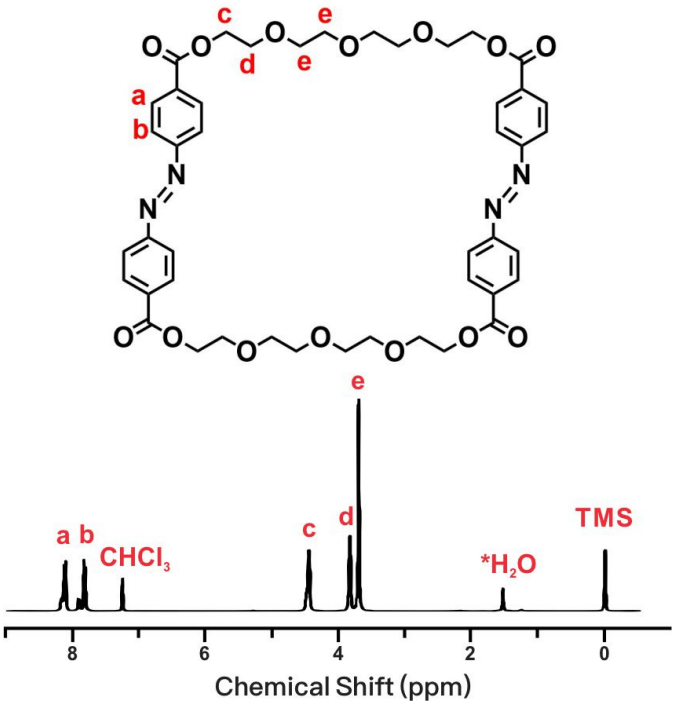


**Figure 1.** Chemical structure and $^{1}$H-NMR spectrum of CDTA. The peak marked with an asterisk corresponds to residual water in the NMR solvent.

NMR spectra were obtained on an Agilent Direct-Drive II 400 MHz NMR spectrometer (Agilent Technologies, Santa Clara, CA, USA). The chemical shifts ($\delta$ values) were measured in parts per million (ppm) down-field from tetramethylsilane (TMS) as an internal reference.

Differential Scanning Calorimetry (DSC) measurements were carried out on a TA Q 200 instrument (TA Instruments, New Castle, DE, USA) with nitrogen as purge gas. Aluminum sample pans were used.

Polarized Optical Microscopy (POM) observations were carried out on a polarizing microscope (BX51-P, Olympus Corporation, Tokyo, Japan) which was coupled with a computer-controlled video camera. A dual hot stage (THMS600, Linkam, Redhill, UK) was used for controlling the temperature.

Small-Angle X-ray Scattering (SAXS) experiments were carried out on an X-ray scattering instrument (SAXSess mc$^2$, Anton Paar, Graz, Austria) equipped with line collimation and a 2200 W sealed-tube X-ray generator (Cu-K$\alpha$, $\lambda$ = 0.154 nm). Samples were wrapped in aluminum foil for SAXS experiments. The sample was kept under vacuum during irradiation. An imaging plate was used to record the scattering pattern. Silver behenate was used as the calibration standard.

## 3. Results and Discussion

### *3.1. Photophysical Properties of CDTA*

The UV-Vis absorption spectrum of CDTA in dichloromethane with concentration of $1.0 \times 10^{-2}$ mg/mL (Figure 2) shows a primary absorption peak at approximately 335 nm in its initial state (predominantly *trans* isomer). Upon irradiation with 365 nm UV light for 30 s, the absorption intensity at this peak decreased to 77.2% of its original value, indicating successful *trans*-to-*cis* photoisomerization. The peak position remained largely unchanged, consistent with the behavior of some cyclic azobenzene derivatives. Concurrently, a slight but discernible increase in absorbance was observed in the 400–500 nm region (inset of Figure 2), corresponding to the characteristic absorption band of the *cis* isomer. Such a weak *cis* absorption band is typical of certain cyclic azobenzene derivatives, at-

tributable to their constrained molecular geometry and modified electronic structure [25,26]. Moreover, the spectral changes were fully reversible under ambient light, and the sample could undergo multiple UV/vis cycles without degradation, further confirming the photoisomerization mechanism.

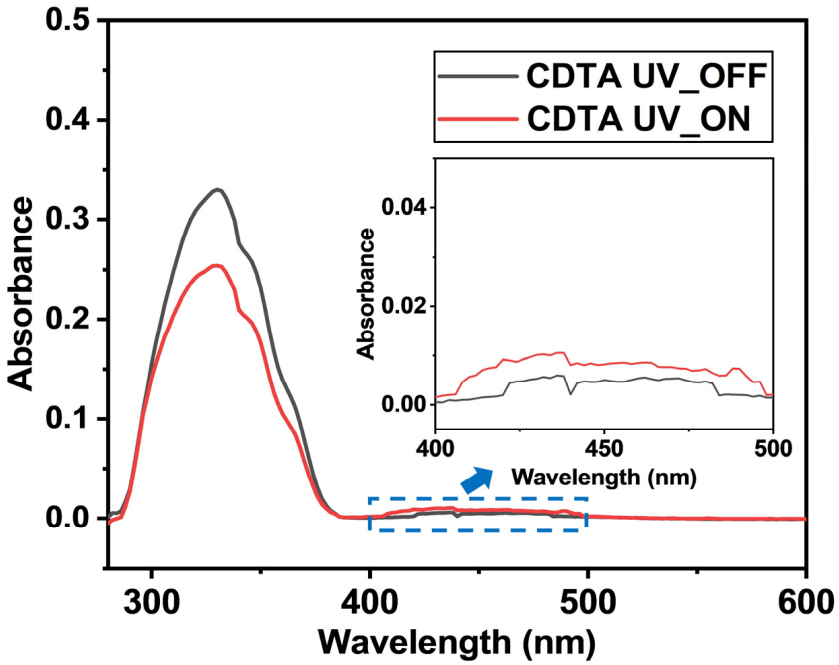


**Figure 2.** UV-Vis absorption spectrum of CDTA in dichloromethane before (black) and after (red) UV irradiation.

### *3.2. Phase Behavior of CDTA*

The phase transition behavior of the pure CDTA compound was investigated using DSC and POM. The DSC thermogram (Figure 3) revealed a complex phase sequence. During the first cooling scan, three exothermic peaks were observed at approximately 169 °C, 144 °C, and 64 °C. These correspond to the transition from the isotropic to a liquid crystalline (LC) phase, from the LC phase to a crystalline state, and between different crystalline states, respectively. The subsequent heating scan showed multiple endothermic events below 165 °C, indicating solid–solid transitions, followed by a clear transition at 165 °C (crystalline to LC) and finally at 179 °C (LC to isotropic).

POM observations were conducted to visually confirm these phases and their characteristic textures. Figure 4 presents POM images of CDTA captured at key temperatures during a slow cooling process (2 °C/min). As shown in Figure 4a, the POM viewfield at 185 °C is completely dark. This darkness under crossed polarizers is the definitive signature of an isotropic state, where the molecular orientation is random and possesses no long-range directional order, resulting in no birefringence. Upon cooling to 165 °C, a well-developed, classic focal conic texture emerges (Figure 4b). This texture is characteristic of a smectic phase, where the molecules are arranged in layers. The distinct birefringence colors and the focal conic domains confirm the formation of a highly ordered LC phase upon transition from the isotropic melt. Further cooling to 140 °C leads to a dramatic change (Figure 4c). The fluid, birefringent texture is replaced by a rigid, non-fluid morphology with sharp, irregular boundaries and altered birefringence patterns. This signifies the transition from the liquid crystalline state to a crystalline solid, accompanied by a loss of molecular mobility.

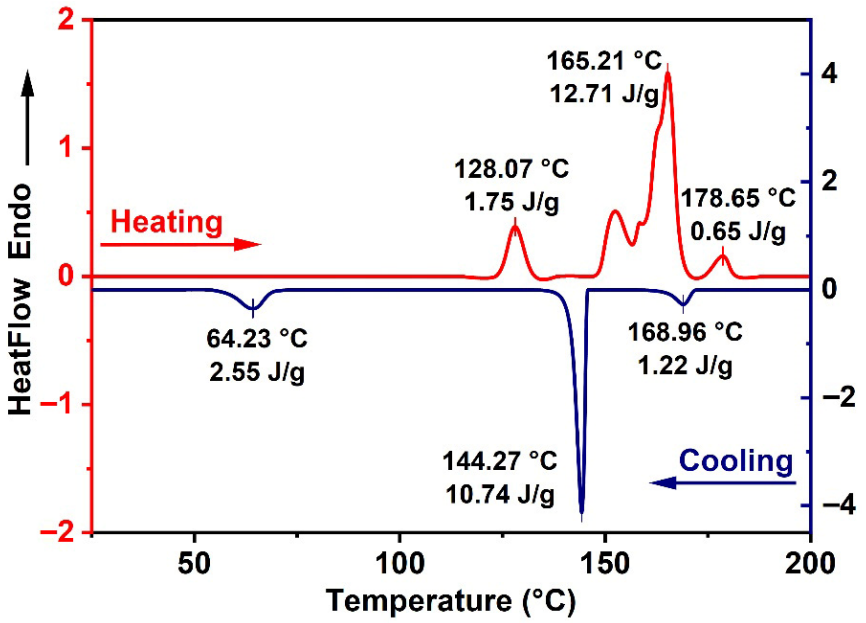


**Figure 3.** DSC curves of pure CDTA upon heating (red) and cooling (navy). Heating/cooling rate: 10 °C/min.

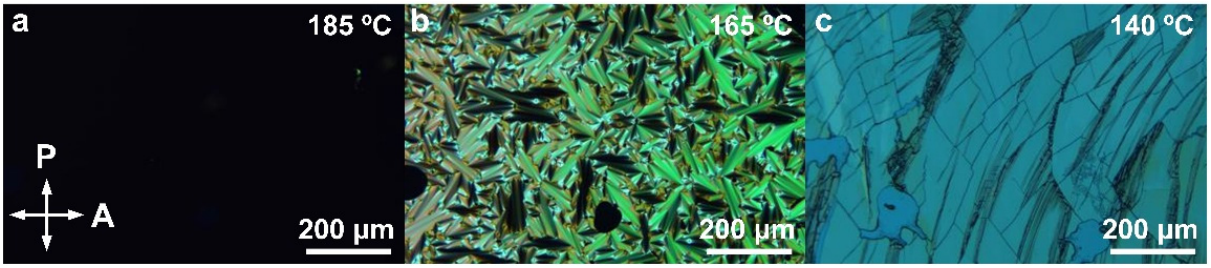


**Figure 4.** POM images of CDTA at different temperatures. (**a**) 185 °C (isotropic state), (**b**) 165 °C (LC state), and (**c**) 140 °C (crystalline state).

To probe the photo-responsiveness within its LC phase, a 10 µm thick cell containing pure CDTA was maintained at 165 °C. Under POM, the initial focal conic texture was clearly visible (Figure 5a). Upon exposure to 365 nm UV light, this texture began to fade rapidly as the sample transitioned towards an isotropic state driven by *trans*-to-*cis* photoisomerization (Figure 5b). After only 2 s of irradiation, the birefringent texture completely vanished, leaving a dark field of view (Figure 5c), indicative of a full photo-induced LC-to-isotropic phase transition. Remarkably, upon cessation of UV light, the dark field reverted to the original focal conic texture (Figure 5d) within a short period under ambient light, demonstrating a fully reversible, photo-driven phase transition cycle facilitated by the azobenzene units.

The molecular packing and structural order of CDTA were further elucidated using SAXS. Figure 6 shows the SAXS profile of CDTA measured at 165 °C, a temperature identified within its crystalline region by DSC and POM. The presence of multiple, integer-ordered Bragg reflections confirms a highly ordered smectic phase with long-range layer periodicity. This structural finding is in perfect agreement with the POM observation of a classic focal conic texture (Figure 4b), which is typical for smectic phases when the layers are curved into focal conic domains. The calculated *d*-spacing of 2.60 nm provides insight into the molecular arrangement of CDTA within the smectic layers. Using *Materials Studio*, molecular modeling of the *trans*-azobenzene unit in its fully extended conformation yields a length of approximately 1.5 nm for the rigid azobenzene core along its long molecular

axis (see Figure S2 in Supplementary Materials). The observed *d*-spacing of 2.60 nm is significantly larger than this value, indicating that the layer spacing is not determined solely by the rigid azobenzene units. Instead, the flexible oligo(ethylene glycol) chains connecting the two azobenzene moieties contribute substantially to the effective molecular length within the smectic layers. In a monolayer smectic A (SmA) arrangement, the rigid azobenzene cores align perpendicular to the layer planes, while the flexible chains extend or adopt conformations that fill the remaining space, resulting in a total layer spacing of 2.60 nm. This interpretation is consistent with the molecular model and supports the proposed SmA phase structure.

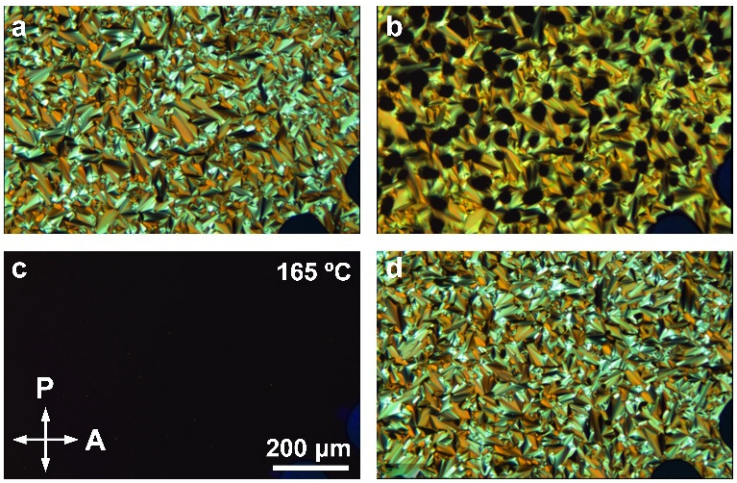


**Figure 5.** Photo-induced reversible phase transition of CDTA in its LC state at 165 °C. (**a**) The characteristic focal conic texture observed under POM without UV irradiation. (**b**) Initiation of texture fading upon exposure to 365 nm UV light. (**c**) Complete disappearance of birefringence after 2 s of UV irradiation. (**d**) Recovery of the original fan-shaped texture after the removal of UV light.

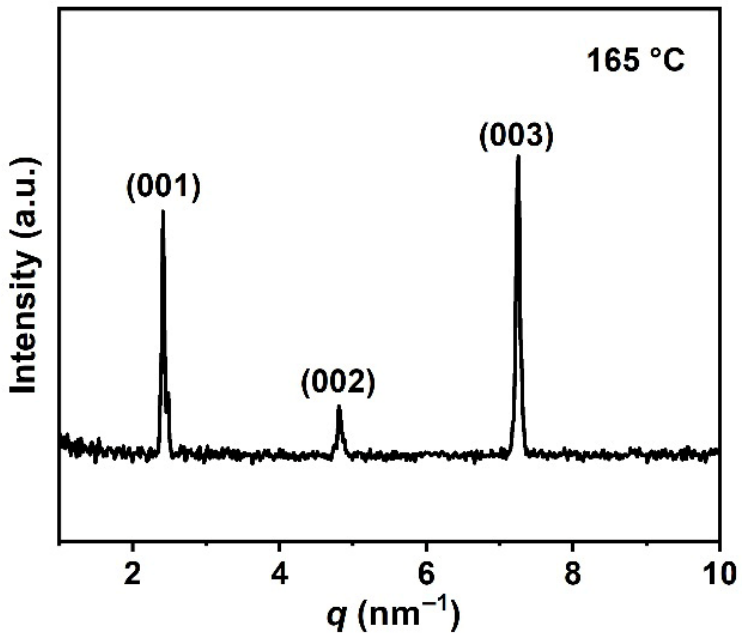


**Figure 6.** SAXS pattern of CDTA in its liquid crystalline state at 165 °C.

It is worth noting that in the SAXS pattern of CDTA (Figure 6), the scattering intensity of the (003) reflection is notably higher than that of the (001) and (002) reflections. This intensity distribution deviates from the typical behavior of conventional smectic A phases,

where the intensity usually decreases with increasing order of reflection. However, the intensity of SAXS reflections is not universally required to follow this trend; rather, it is determined by the Fourier transform of the electron density distribution along the layer normal. For molecules with non-uniform electron density profiles—such as CDTA, which contains rigid, electron-rich azobenzene cores and flexible, electron-deficient oligo(ethylene glycol) chains—the molecular form factor can selectively enhance certain higher-order reflections. In our case, the enhanced (003) reflection likely arises from this specific electron density modulation within the layer, a phenomenon that has been observed in other liquid crystalline systems with complex molecular architectures [39,40]. This interpretation is consistent with the cyclic structure of CDTA and further supports the proposed smectic A phase assignment.

### *3.3. Phase Behavior of the Host Liquid Crystal 8CB*

The phase behavior of the host liquid crystal 8CB, which is well-documented in the literature, was characterized for reference [41]. As confirmed by DSC and SAXS (Figure 7), 8CB exhibits a smectic A (SmA) phase at room temperature and below, transitioning to a nematic (N) phase upon heating. The smectic-to-nematic transition temperature was found at approximately 29 °C, while the nematic-to-isotropic transition occurred near 43 °C. SAXS at 20 °C showed a sharp peak corresponding to a layer spacing of 3.14 nm, characteristic of the SmA phase (Figure 7b).

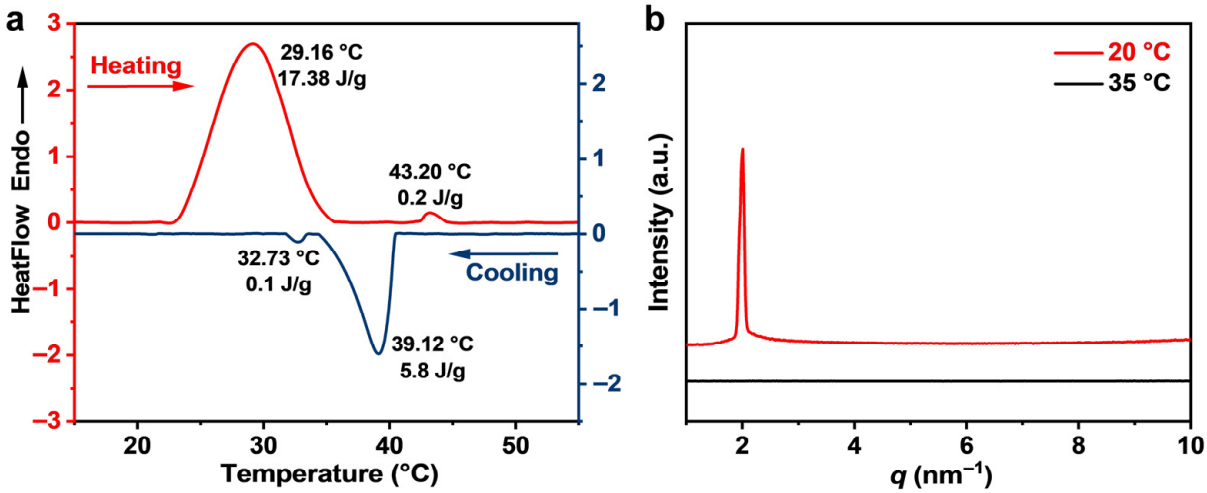


**Figure 7.** Phase behavior characteristics of 8CB. (**a**) DSC; (**b**) SAXS.

For clarity, the phase transition temperatures and corresponding phase assignments for CDTA and 8CB are summarized in Table 1. For the CDTA/8CB composites, due to the low dopant concentration (≤2.5 wt%), the thermal signals from CDTA are negligible in DSC measurements and completely overshadowed by the dominant 8CB matrix. The phase sequence of the composites is thus expected to be the same as that of 8CB.

**Table 1.** Phase sequences of CDTA and 8CB.

| Sample | Phase Sequences [1] |
|---|---|
| CDTA | Heating: Cr1 128 (1.75) Cr2 165 (12.71) SmA 179 (0.65) Iso<br>Cooling: Iso 169 (1.22) SmA 144 (10.74) Cr2 64 (2.55) Cr1 |
| 8CB | Heating: SmA 29 (17.38) N 43 (0.2) Iso<br>Cooling: Iso 39 (5.8) N 33 (0.1) SmA |

[1] Phase transition temperatures (°C) and enthalpies (J/g, given in parentheses) determined by DSC. Iso: isotropic liquid; SmA: smectic A; N: nematic; Cr: crystal.

### *3.4. Photo-Responsive Behavior of CDTA/8CB Composites*

To systematically investigate the influence of dopant concentration on the photo-response, three composite mixtures of CDTA and the host liquid crystal 8CB were prepared with the following weight ratios: 98.5:1.5, 98:2, and 97.5:2.5. These mixtures are denoted as 1.5 wt%, 2.0 wt%, and 2.5 wt% CDTA composites, respectively.

The photo-induced transmittance modulation of the composites was quantitatively characterized using a custom-built optical setup, as schematically illustrated in Figure 8. A halogen cold light source (1) provided a collimated beam. The beam was shaped by an aperture (3) after passing through a convex lens (2). The test cell (4) containing the composite was placed in the beam path. The transmitted light was then collected and focused by another convex lens (5) onto a fiber-optic receiver (6) connected to a spectrometer (7). This setup allowed for real-time monitoring of the spectral transmittance, with a specific focus on the 630 nm wavelength, under controlled UV illumination. The response times for photo-induced switching were defined as the time required to complete 90% of the total transmittance change upon UV irradiation or during recovery under ambient light.

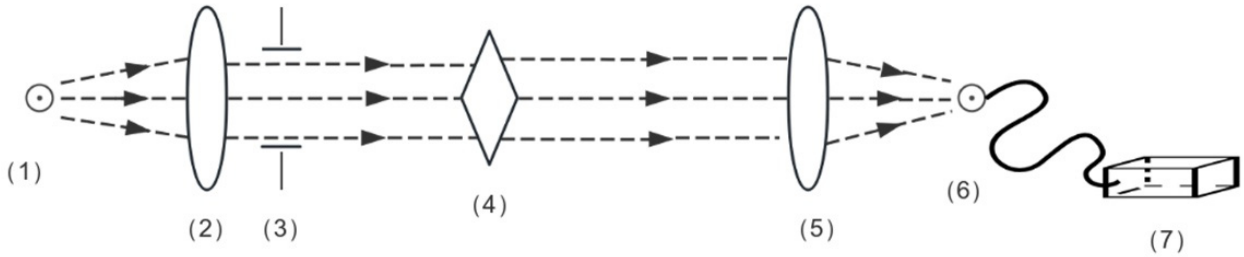


**Figure 8.** Schematic of the optical setup for real-time transmittance measurement. (1) Light source, (2, 5) Convex lenses, (3) Aperture, (4) LC test cell, (6) Optical receiver, (7) Spectrometer.

Figure 9 details the real-time transmittance switching curves at 630 nm for the three composites at 25 °C, under alternating cycles of 365 nm UV exposure and ambient light recovery. For the 1.5 wt% composite, UV irradiation for ~253.9 s induced a *trans*-to-*cis* isomerization, increasing the transmittance by ~11% before recovery within 27.1 s. The 2.0 wt% composite required ~312.5 s of UV exposure to achieve a maximum transmittance increase from 51% to 63.4% ($\Delta T \approx 12.4\%$), with a recovery time of 47.6 s. The 2.5 wt% composite exhibited the fastest UV response (~134.8 s) and also the most rapid recovery (26.3 s). The results indicate a non-monotonic relationship between dopant concentration and response kinetics, governed by competing factors such as increased photo-switch density and potential aggregation or altered free volume.

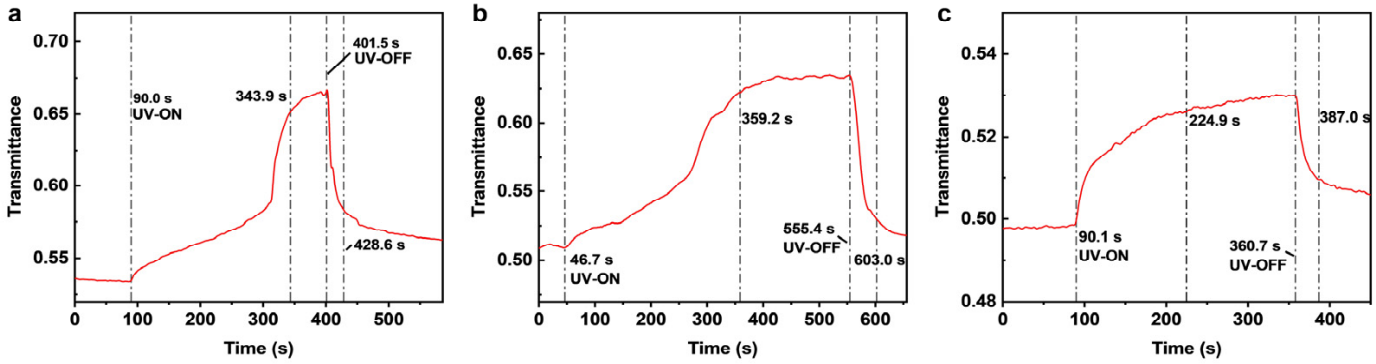


**Figure 9.** Real-time transmittance kinetics of CDTA/8CB composites with different ratios at 630 nm under UV cycling at 25 °C. (**a**) 1.5 wt%; (**b**) 2.0 wt%; (**c**) 2.5 wt%.

The increase in transmittance upon UV irradiation can be explained by the following mechanism. The *trans*-to-*cis* photoisomerization of the azobenzene units in CDTA generates bent *cis* isomers that are geometrically incompatible with the orientational order of the host 8CB liquid crystal. This incompatibility disrupts the local molecular alignment, inducing a partial or complete phase transition from the highly scattering liquid crystalline state to a more transparent isotropic state. The resulting reduction in refractive index inhomogeneities within the cell decreases light scattering and consequently increases the forward transmittance. Upon removal of UV light, visible light-driven *cis*-to-*trans* back-isomerization restores the original rod-like trans geometry, allowing the LC order to recover and the transmittance to return to its initial low level. This reversible order–disorder transition is the fundamental mechanism underlying the photo-switching behavior observed in Figure 9.

While the 2.5 wt% composite showed the fastest response kinetics, the 2.0 wt% composite offered the optimal balance between a significant transmittance modulation ($\Delta T$) and a reasonable response time. Therefore, the 2.0 wt% composite was selected for subsequent detailed investigations, as its larger $\Delta T$ is more critical for practical applications in light modulation.

Given that the photo-response is coupled to the order–disorder transition of the host LC matrix, the kinetics are profoundly influenced by temperature. Figure 10 presents the transmittance switching for the optimized 2.0 wt% composite at two representative temperatures within the nematic phase and near the smectic–nematic transition of the host 8CB. The corresponding behavior at 25 °C (smectic phase) is shown in Figure 9b.

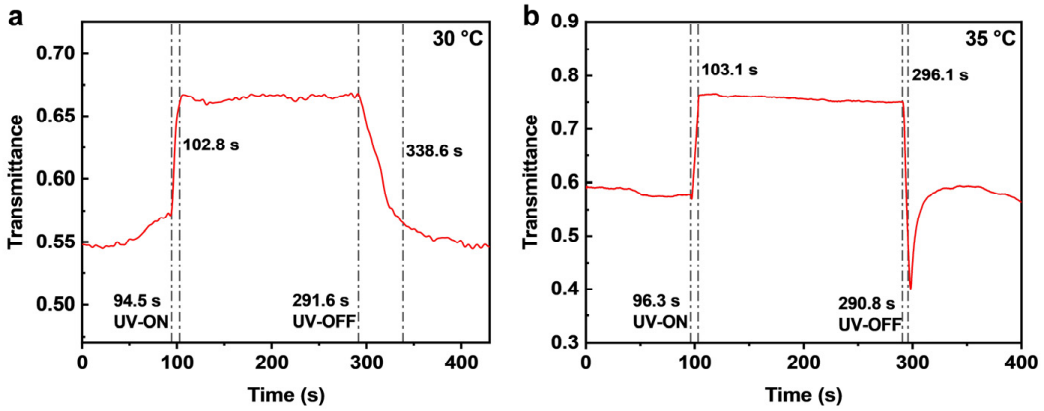


**Figure 10.** Temperature dependence of the photo-response for the 2.0 wt% CDTA/8CB composite. (**a**) 30 °C; (**b**) 35 °C.

At 25 °C (host in SmA phase), the UV response was slow (~312.5 s) due to the high viscosity and stability of the layered structure (Figure 9b). At 30 °C (near the SmA-N transition of 8CB), the response time drastically shortened to ~8.3 s, with a $\Delta T$ of ~12% (Figure 10a). At 35 °C (host in N phase), the response further accelerated to ~6.8 s, yielding the largest transmittance modulation ($\Delta T \approx 18.4\%$, Figure 10b). The dramatic acceleration is attributed to the host's transition to the less ordered, more fluid N phase, which is more susceptible to disorder induced by the conformational change in CDTA.

It is worth noting that the reversibility of the photo-switching process is demonstrated by the single-cycle measurements in Figures 9 and 10, where the transmittance returns to its initial level after removal of UV light for each composite concentration. This functional reversibility is further supported by the POM observations in Figure 5, which show a complete and reversible photo-induced phase transition for pure CDTA. Together, these results confirm that the *cis*-to-*trans* back-isomerization occurs efficiently under ambient

light, enabling repeated use of the material without noticeable fatigue in a single cycle. Systematic investigation of long-term cycling stability will be addressed in future studies.

The visual effect of this photo-modulation is demonstrated in Figure 11. A patterned card viewed through the 2.0 wt% CDTA/8CB composite cell in the initial *trans*-dominant state was hazy. After 400 s of UV irradiation, with *cis*-dominant state formed in the cell, clear visual field was shown. And after removing UV light, the hazy state was recovered. The light shutter functionality of the composite cell was thus visually confirmed. This reversible clarity switch highlights its application potential for privacy and daylighting control.


**Figure 11.** Visual demonstration of the photo-switching capability. The background of the liquid crystal cells is the emblem of the authors' university, and the non-English characters indicate the Chinese name of the university.

To contextualize the performance of the cyclic CDTA within the broader field of azobenzene-doped liquid crystals, it is instructive to compare our results with those reported for linear azobenzene derivatives. Typical linear azobenzene-doped LC systems exhibit response times ranging from seconds to minutes depending on concentration, temperature, and molecular structure [20,21]. The slower response observed for CDTA at room temperature (>300 s) can be attributed to its cyclic structure, which imposes conformational constraints on the azobenzene units. In the highly ordered smectic phase of 8CB, these constraints may reduce the efficiency of isomerization-induced perturbation, leading to slower kinetics compared to more flexible linear analogs. However, this structural rigidity also offers potential advantages, such as enhanced thermal stability of the *cis* isomer and a more pronounced steric effect once isomerization occurs. These comparisons suggest that the cyclic architecture introduces a trade-off between response speed and modulation depth, which could be exploited for specific applications requiring either rapid switching or high contrast.

### *3.5. Photoelectrical Responsive Properties of the Composites*

To achieve versatile control suitable for smart window applications, the ability to modulate light transmission via both optical and electrical stimuli is highly advantageous. Beyond the photo-responsive behavior, the electro-optical switching capability of the CDTA/8CB composites was thoroughly investigated. The transmittance at 630 nm was monitored under an applied DC electric field, revealing a critical dependence on the phase state of the host 8CB matrix.

At 25 °C, where the host 8CB is in the highly ordered and viscous smectic A (SmA) phase, applying a voltage up to 10 V resulted in no measurable change in transmittance (Figure 12a). This absence of response is attributed to the strong layer constraints and high rotational viscosity of the SmA phase, which effectively suppress large-scale reorientation of the LC directors under the applied field. In contrast, at 35 °C where 8CB is in the nematic (N)

phase, a pronounced electro-optical response was observed (Figure 12b). The transmittance remained stable at a low level (~51.8%) until a threshold voltage was exceeded. Upon increasing the voltage from 2 V to 10 V, the transmittance increased progressively, reaching a maximum of 79.9% at 10 V. This behavior is characteristic of a field-induced reorientation of the nematic directors. The reorientation reduces the refractive index mismatch within the cell, thereby decreasing light scattering and increasing forward transmittance.

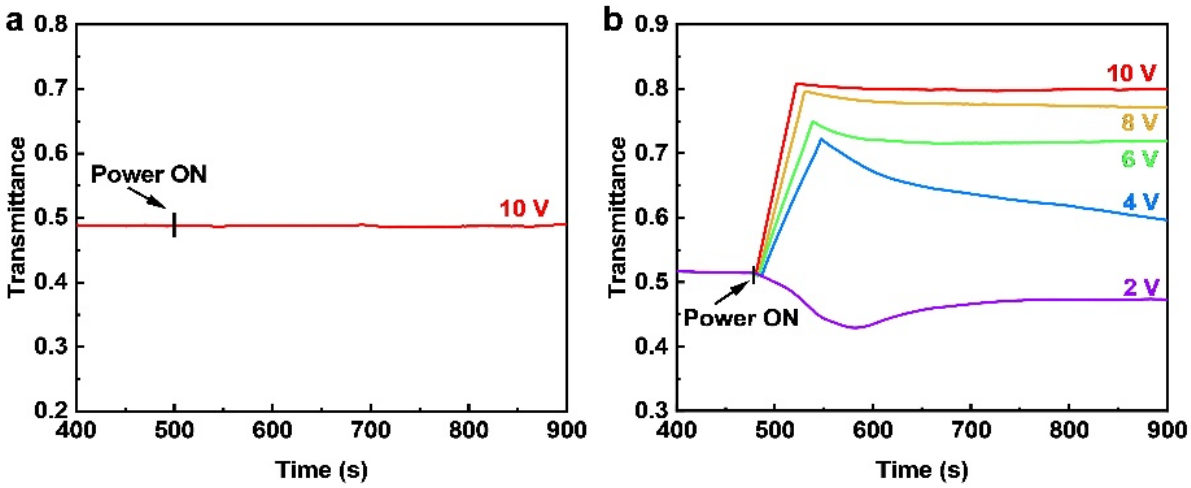


**Figure 12.** Electro-optical response of the 2.0 wt% CDTA/8CB composite at 25 °C (**a**) and 35 °C (**b**).

## 4. Conclusions

In summary, a novel cyclic diazo compound (CDTA) was synthesized and successfully employed as a molecular switch to impart dual photo- and electro-responsiveness to liquid crystal composites. When doped into the well-known host 8CB, the CDTA/8CB composite exhibited a pronounced, reversible photo-induced increase in visible light transmittance upon exposure to 365 nm UV irradiation. This effect is driven by the *trans*-to-*cis* isomerization of the azobenzene units in CDTA, which disrupts the order of the host LC matrix. The response kinetics were found to be intricately dependent on both dopant concentration and temperature. An optimal dopant concentration of 2.0 wt% was identified, offering a significant transmittance change ($\Delta T$). Most notably, the UV response time was dramatically accelerated from over 300 s at 25 °C to merely 6.8 s at 35 °C. This marked acceleration is directly correlated with the host's phase transition from the highly ordered, viscous smectic A phase to the more fluid nematic phase, which is far more susceptible to photo-induced disorder.

Furthermore, the composite demonstrated complementary electro-optical switching in its nematic state, with transmittance effectively modulated by an applied DC electric field. This work elucidates a clear design principle: the photo-response is governed by the guest molecular switch (CDTA), while the electro-response is dictated by the phase characteristics of the host LC matrix. This decoupling enables independent control pathways. The developed composite, with its dual-stimuli responsiveness and tunable kinetics, presents a promising and versatile platform for next-generation smart windows capable of autonomous adaptation to ambient light and temperature, coupled with on-demand user control via electricity. Future work will focus on molecular engineering of the cyclic azobenzene structure to further enhance the response speed, contrast ratio, and spectral range of modulation, particularly extending into the near-infrared region for optimal energy-saving performance. Long-term cycling stability and durability under repeated on–off switching will also be systematically evaluated to assess the material's suitability for practical applications.

**Supplementary Materials:** The following supporting information can be downloaded at: https://www.mdpi.com/article/10.3390/photonics13040331/s1, Figure S1: Synthetic route of cyclic diazo compound CDTA; Figure S2: Molecular model of the *trans*-azobenzene unit in its fully extended conformation, obtained using *Materials Studio*.

**Author Contributions:** Conceptualization, H.L. and Z.C.; methodology, H.S. and C.M.; chemical synthesis, T.S. and Y.W.; characterization, T.S., B.Z. and N.S.; data curation, T.S.; writing—original draft preparation, T.S.; writing—review and editing, H.L. All authors have read and agreed to the published version of the manuscript.

**Funding:** This research was funded by National Key Research and Development Program of China (2023YFB3209200); China Postdoctoral Science Foundation (2024M762317); Open Project of Key Laboratory of Green Chemical Engineering Process of Ministry of Education (GCP2025007).

**Institutional Review Board Statement:** Not applicable.

**Data Availability Statement:** The data that support the findings of this study are available from the corresponding authors upon reasonable request.

**Conflicts of Interest:** The authors declare no conflicts of interest.

## Abbreviations

The following abbreviations are used in this manuscript:

| | |
|---|---|
| DSC | Differential Scanning Calorimetry |
| POM | Polarized Optical Microscopy |
| LC | Liquid Crystal |
| SmA | Smectic A |
| N | Nematic |

## References

1. Mutoh, K.; Miyashita, N.; Arai, K.; Abe, J. Turn-On Mode Fluorescence Switch by Using Negative Photochromic Imidazole Dimer. *J. Am. Chem. Soc.* **2019**, *141*, 5650–5654. [CrossRef]
2. Mutoh, K.; Kobayashi, Y.; Nakashima, T. A Hexaarylbiimidazole-Terarylene Hybrid: Visible-to-NIR-II Absorption via Sequential Photochromic Reactions. *Angew. Chem. Int. Ed.* **2024**, *63*, e202410115. [CrossRef] [PubMed]
3. Moriyama, N.; Yagi, S.; Abe, J. Stepwise Photochromism of Large Macrocycles Incorporating Two Negative Photochromic Units. *J. Phys. Chem. Lett.* **2024**, *15*, 7548–7555. [CrossRef]
4. Shallcross, R.C.; Zacharias, P.; Köhnen, A.; Körner, P.O.; Maibach, E.; Meerholz, K. Photochromic Transduction Layers in Organic Memory Elements. *Adv. Mater.* **2013**, *25*, 469–476. [CrossRef]
5. Xu, C.; Zhang, J.; Xu, W.; Tian, H. Multifunctional Organic Field Effect Transistors Constructed with Photochromic Molecules. *Mater. Chem. Front.* **2021**, *5*, 1060–1075. [CrossRef]
6. Kawanishi, Y.; Segawa, Y.; Mutoh, K.; Abe, J.; Kobayashi, Y. A Photochromic Carbazolyl-Imidazolyl Radical Complex. *Chem. Commun.* **2022**, *58*, 4997–5000. [CrossRef]
7. Thaggard, G.C.; Kankanamalage, B.K.P.M.; Lim, J.; Shi, X.; Arnold, V.S.; Badiger, M.; Mulkerrin, R.; Broskey, R.D.; Irizarry, E.; Atim, G.; et al. Altering the Thermodynamics of Stimuli-Responsive Derivatives through Layered Hybrid Material Design. *J. Am. Chem. Soc.* **2025**, *147*, 42591–42606. [CrossRef]
8. Li, G.; Hatano, R.; Maisonneuve, S.; Iimura, K.; Kim, Y.; Xie, J. Azobenzene-Based Glycomacrocycles: Synthesis, Photoisomerization, and Photomodulation of Liquid Crystal Helical Pitch with Helix Inversion. *Chem. Eur. J.* **2025**, *31*, e02131. [PubMed]
9. Wang, G.; Zhang, M.; Yang, Q.; Liu, F.; Cheng, Z.; Guo, R.; Yang, H. Photoinduced Phase Transitions in Chiral Binaphthyl-diol-doped Smectic Liquid Crystals by a Photochromic Azobenzene. *Chem. Lett.* **2010**, *39*, 1144–1145. [CrossRef]
10. Bugakov, M.; Shibaev, V.; Boiko, N. Substituent Polarity Effect and Holographic Grating Recording in Thin Films of Azobenzene-Containing Liquid Crystalline Polymers. *Opt. Mater.* **2026**, *169*, 117661.
11. Arago, G.; Glüsenkamp, K.H.; Haberhauer, G. Multistate Azobenzene-Norbornadiene Photoswitches for Molecular Solar Thermal Energy Storage. *Chem. Eur. J.* **2026**, *32*, e02520. [CrossRef]
12. He, J.; Wei, M.; Chen, Y.T.; Phillips, D.L.; Dang, L.; Li, M.D. From Molecule to Nanocrystalline: Ultrafast Dynamics of *trans-cis* Isomerization of Azobenzene Derivatives. *Phys. Chem. Chem. Phys.* **2025**, *27*, 24104–24111. [CrossRef]

13. Ovalle, M.; Doellerer, D.; Feringa, B.L. Azobenzene-Oxindole Photochromic Dyads. *Angew. Chem. Int. Ed.* **2025**, *64*, e202501872. [CrossRef]
14. Yan, Y.; Zhang, K.; Sun, L.; Zhang, Q.; Meng, Y.; Cheng, H.; Zhang, X.; Zhao, R.; Liu, F. A Smart Nanofiber Film Based Azobenzene Moiety with Reversible Photoresponsive Patterning Ability for Information Storage. *Dye. Pigment.* **2025**, *240*, 112834. [CrossRef]
15. Hsieh, H.C.; Chen, P.W.; Su, C.Y.; Chen, Y.H.; Wang, C.S.; Yeh, M.Y. Substituent Effects on Shape-Memory and Photoisomerization in $\beta$-Cyclodextrin-Azobenzene Composite Gels. *Chem. Mater.* **2025**, *37*, 8677–8687. [CrossRef]
16. Quinchia, J.; Cruz-Pacheco, A.F.; Ruiz-Molina, D.; Orozco, J. Dual Responsive Polymersomes as Versatile, Intelligent Labeling System in Biosensing. *Chem. Eng. J.* **2024**, *500*, 157165. [CrossRef]
17. Yoon, W.J.; Lim, S.I.; Rim, M.; Koo, J.; Ko, H.; Jang, J.; Oh, M.; De Sio, L.; Choi, Y.J.; Jeong, K.U. Photo- and Thermo-Responsive Switchable Smart Windows Developed by the Control of 3D Molecular Orientation of Chiral Liquid Crystals with Azobenzene Molecular Engineering. *Adv. Funct. Mater.* **2025**, *35*, 2425115. [CrossRef]
18. Meng, X.; Lin, S.; Chen, S.; Shen, X.; Guo, D.; Guo, J. Recent Advances in Smart Windows Based on Photo-Responsive Liquid Crystals Featuring Phase Transition. *ChemPlusChem* **2024**, *89*, e202300700. [PubMed]
19. Ube, T.; Yoshida, M.; Kurihara, S.; Ikeda, T. Sunlight-Driven Smart Windows with a Wide Temperature Range of Optical Switching Based on Chiral Nematic Liquid Crystals. *ACS Appl. Mater. Interfaces* **2024**, *16*, 28638–28644. [CrossRef] [PubMed]
20. Oh, S.W.; Nam, S.M.; Kim, S.H.; Yoon, T.H.; Kim, W.S. Self-Regulation of Infrared Using a Liquid Crystal Mixture Doped with Push-Pull Azobenzene for Energy-Saving Smart Windows. *ACS Appl. Mater. Interfaces* **2021**, *13*, 5028–5033. [CrossRef] [PubMed]
21. Han, C.H.; Lee, J.H.; An, C.H.; Oh, S.W. A Liquid Crystal Smart Window for Energy Saving and Harvesting. *Appl. Mater. Today* **2023**, *35*, 101923. [CrossRef]
22. Tkachenko, I.M.; Kurioz, Y.I.; Kravchuk, R.M.; Kobzar, Y.L.; Litoshenko, D.V.; Glushchenko, A.V.; Shevchenko, V.V.; Nazarenko, V.G. Photoinduced Birefringence and Liquid Crystal Orientation on Polymers with Different Azobenzene Content in the Main Chain. *ACS Appl. Mater. Interfaces* **2024**, *16*, 52945–52957. [CrossRef]
23. Chen, B.; Wang, Z.; Lu, J.; Yang, X.; Wang, Y.; Zhang, Z.; Zhu, J.; Zhou, N.; Li, Y.; Zhu, X. Cyclic Azobenzene-Containing Amphiphilic Diblock Copolymers: Solution Self-Assembly and Unusual Photo-Responsive Behaviors. *Polym. Chem.* **2015**, *6*, 3009–3013. [CrossRef]
24. Norikane, Y.; Kitamoto, K.; Tamaoki, N. [1.1](3,3′)-Azobenzenophane: Novel Crystal Structure and Cis-Trans Isomerization of Distorted Azobenzene. *Org. Lett.* **2002**, *4*, 3907–3910. [CrossRef] [PubMed]
25. Siewertsen, R.; Neumann, H.; Buchheim-Stehn, B.; Herges, R.; Näther, C.; Renth, F.; Temps, F. Highly Efficient Reversible Z-E Photoisomerization of a Bridged Azobenzene with Visible Light through Resolved $S_1(n\pi^*)$ Absorption Bands. *J. Am. Chem. Soc.* **2009**, *131*, 15594–15595. [CrossRef] [PubMed]
26. Lu, H.B.; Xie, X.Y.; Xing, J.; Xu, C.; Wu, Z.Q.; Zhang, G.B.; Lv, G.Q.; Qiu, L.Z. Wavelength-Tuning and Band-Broadening of a Cholesteric Liquid Crystal Induced by a Cyclic Chiral Azobenzene Compound. *Opt. Mater. Express* **2016**, *6*, 3145–3158. [CrossRef]
27. Norikane, Y.; Kitamoto, K.; Tamaoki, N. Novel Crystal Structure, Cis-Trans Isomerization, and Host Property of Meta-Substituted Macrocyclic Azobenzenes with the Shortest Linkers. *J. Org. Chem.* **2003**, *68*, 8291–8304. [CrossRef]
28. Norikane, Y.; Hiraib, Y.; Yoshida, M. Photoinduced Isothermal Phase Transitions of Liquid-Crystalline Macrocyclic Azobenzenes. *Chem. Commun.* **2011**, *47*, 1770–1772. [CrossRef]
29. Takaishi, K.; Muranaka, A.; Kawamoto, M.; Uchiyama, M. Photoinversion of Cisoid/Transoid Binaphthyls. *Org. Lett.* **2012**, *14*, 276–279. [CrossRef]
30. Reuter, R.; Wegner, H.A. Switchable 3D Networks by Light Controlled $\pi$-Stacking of Azobenzene Macrocycles. *Chem. Commun.* **2013**, *49*, 146–148. [CrossRef] [PubMed]
31. Peng, J.; Zuo, C.; Xiao, Q.; Deng, K.; Meng, C.; Liu, Y.; Zhang, M.; Ma, L.; Pun, S.H.; Wei, H. Synthesis of Stimuli-Responsive Nanosized Ring-Like Colloids and Cyclic Polymers via A Dual-Template Approach. *Chem. Sci.* **2019**, *10*, 3943–3948. [PubMed]
32. Ramos-Soriano, J.; Jiang, Y.J.; Deng, B.; O'Hagan, M.P.; Rao, A.G.; Lu, D.; Haldar, S.; Oliveira, A.S.F.; Mulholland, A.J.; Galan, M.C. Bridged Azobenzene Exhibits Fully Reversible Photocontrolled Binding to a G-Quadruplex DNA/Duplex Junction. *JACS Au* **2025**, *5*, 3846–3857. [CrossRef] [PubMed]
33. Niu, Q.; Li, D.; Guo, L.; Sun, X.; Liu, Y.; Cheng, L.; Jin, B. Ten-Membered Cyclic Azobenzene: Electrochemical Synthesis and Photochromic Properties. *ChemElectroChem* **2025**, *12*, e202500111. [CrossRef]
34. Sun, X.; Li, D.; Niu, Q.; Liu, Y.; Zhang, D.; Cheng, L.; Jin, B. Electrochemical Synthesis and Photochromic Properties of Eight-Member Cyclic Azobenzenes. *Electrochim. Acta* **2025**, *526*, 146172. [CrossRef]
35. Liu, Z.; Zhang, C.; Li, S.; Zhou, Y.; Lan, F.; Zhao, X.; Su, Z.; Hu, C.; Deng, P.; Yu, Z. Light-intersecting Photoclick Reactions for Bioorthogonal Labeling on Single Cells: Dibenzo[*b*,*f*][1,4,5]thiadiazepine-11,11-dioxide as a Photoswitchable Reporter. *Angew. Chem. Int. Ed.* **2025**, *64*, e202501936. [CrossRef]
36. Zhou, M.; Lu, H.; Zhang, X.; Zhang, Q.; Xu, M.; Zhu, J.; Zhang, G.; Ding, Y.; Qiu, L. Tuning Helical Twisting Power and Photoisomerisation Kinetics of Axially Chiral Cyclic Azobenzene Dopants in Cholesteric Liquid Crystals. *Liq. Cryst.* **2019**, *46*, 2181–2189. [CrossRef]

37. Wang, H.; Bisoyi, H.K.; McConney, M.E.; Urbas, A.M.; Bunning, T.J.; Li, Q. Visible-Light-Induced Self-Organized Helical Superstructure in Orientationally Ordered Fluids. *Adv. Mater.* **2019**, *31*, 1902958. [CrossRef] [PubMed]
38. Xiao, Y.; He, C.; Yang, Z.F.; Chen, E.Q.; Lu, H.J.; Li, X.H.; Tu, Y.F. The Shackling Effect in Cyclic Azobenzene Liquid Crystal. *Chin. J. Polym. Sci.* **2022**, *40*, 584–592.
39. Yoon, H.G.; Agra-Kooijman, D.M.; Ayub, K.; Lemieux, R.P.; Kumar, S. Direct Observation of Diffuse Cone Behavior in de Vries Smectic-A and -C Phases of Organosiloxane Mesogens. *Phys. Rev. Lett.* **2011**, *106*, 087801. [CrossRef]
40. Lu, H.; Shi, X.; Hamaguchi, K.; Uchida, J.; Kato, T.; Ungar, G. X-ray Diffraction on Smectic Liquid Crystals: Determining Molecular Arrangement from Diffraction Intensities. *J. Mol. Liq.* **2025**, *423*, 126866. [CrossRef]
41. Sadati, M.; Ramezani-Dakhel, H.; Bu, W.; Sevgen, E.; Liang, Z.; Erol, C.; Rahimi, M.; Qazvini, N.T.; Lin, B.; Abbott, N.L.; et al. Molecular Structure of Canonical Liquid Crystal Interfaces. *J. Am. Chem. Soc.* **2017**, *139*, 3841–3850. [CrossRef] [PubMed]